

Hybrid Filtering Heuristic for the Sensor-Placement Problem to Discretize 2D Continuous Environments

Jan Mikula^{1,2}, Miroslav Kulich¹

Abstract—This paper addresses the sensor-placement problem (SPP) within the context of discretizing large, complex continuous 2D environments into graphs for efficient task-oriented route planning. The SPP aims to minimize the number of sensors required to achieve a user-defined coverage ratio while considering a general visibility model. We propose the hybrid filtering heuristic (HFH) framework, which enhances or combines outputs of existing sensor-placement methods, incorporating a filtering step. This step eliminates redundant sensors or those contributing marginally to the coverage, ensuring the coverage ratio remains within the desired interval. We implement two versions of HFH: the basic version and a variant, HFHB, incorporating a preprocessing technique known as bucketing to accelerate region clipping. We evaluate HFH and HFHB on a dataset of large, complex polygonal environments, comparing them to several baseline methods under both unlimited and limited-range omnidirectional visibility models. The results demonstrate that HFH and HFHB outperform baselines in terms of the number of sensors required to achieve the desired coverage ratio. Additionally, HFHB significantly reduces the runtime of more competitive baseline methods. We also adapt HFHB to a visibility model with localization uncertainty, demonstrating its effectiveness up to a certain level of uncertainty.

Index Terms—Task Planning, Computational Geometry, Reactive and Sensor-Based Planning, Sensor Placement Heuristics.

I. INTRODUCTION

THIS paper addresses a variant of the sensor-placement problem (SPP), which involves strategically positioning static sensors within a known 2D continuous environment. The general objective of the SPP is to ensure the environment is covered by the sensors and to minimize the number of sensors required for this coverage. Coverage is determined by the visible regions from each sensor, as defined by a specified visibility model.

Sensor-placement problems, including variants with various constraints, modified objectives, or extensions to 3D, have applications across a wide range of domains. These domains include urban surveillance systems, environmental monitoring, smart agriculture, and robotics. For instance, sensor placement is crucial for transport network surveillance and general-purpose urban area monitoring [1], [2], health monitoring

This work was co-funded by the European Union under the project Robotics and advanced industrial production (reg. no. CZ.02.01.01/00/22_008/0004590) and by the Grant Agency of the Czech Technical University in Prague, grant no. SGS23/175/OHK3/3T/13.

¹Both authors are with the Czech Institute of Informatics, Robotics and Cybernetics, Czech Technical University in Prague, Jugoslavských partyzánů 1580/3, Prague 6, 16000, Czech Republic.

jan.mikula@cvut.cz, miroslav.kulich@cvut.cz

²Jan Mikula is also with the Department of Cybernetics, Faculty of Electrical Engineering, Czech Technical University in Prague, Karlovo náměstí 293/13, Prague 2, 121 35, Czech Republic.

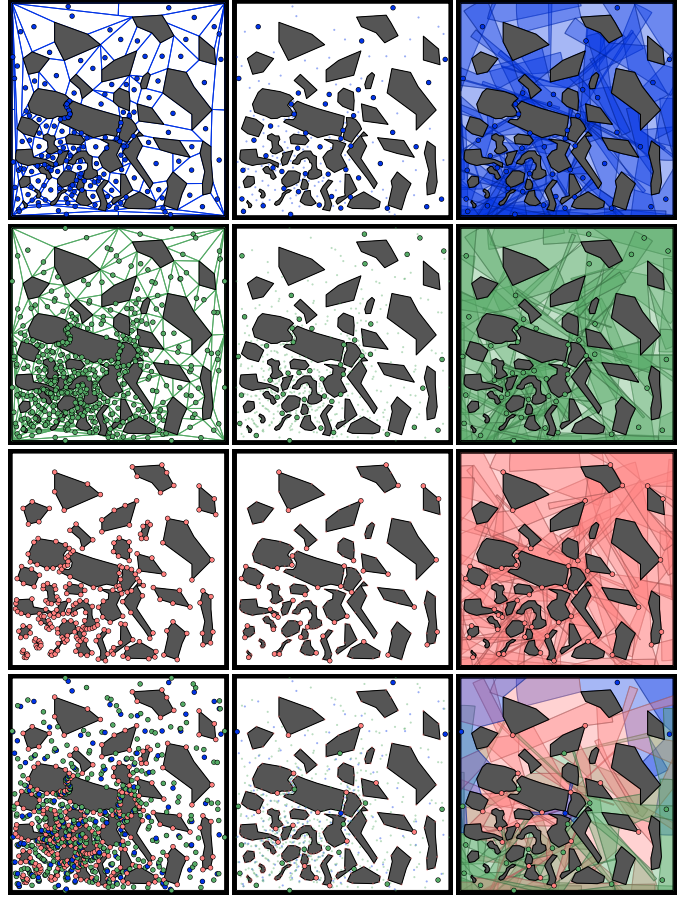


Fig. 1. The two main concepts behind the HFH framework: the filtering step and the combination of outputs from multiple methods. The first column (first to third rows) shows the initial sensor-placement sets generated by the KA (blue), CCDT (green), and RV (pink) baseline methods. The second column presents the filtered sets, while the third column displays the coverage achieved by these filtered sets. The last row illustrates the combined output of the KA, CCDT, and RV methods, along with the filtered set and the coverage achieved. The filtering step results in the following reductions in the number of guards: KA: $161 \rightarrow 46$; CCDT: $403 \rightarrow 45$; RV: $257 \rightarrow 46$; KA,CCDT, RV: $821 \rightarrow 37$. Note that the lowest value achieved after filtering is for the combined method.

of structures such as bridges and buildings [3], and field information coverage in agricultural systems [4]. In robotics, the SPP can be tailored to improve mobile robot navigation [5] or assist in planning efficient inspection routes [6].

This paper specifically addresses the SPP within the following context and considerations:

- **Application Focus:** Discretizing large, complex continuous 2D environments into graphs, where nodes represent sensor locations and edges denote the shortest paths

between them. The purpose of these graphs is to facilitate efficient task-oriented route planning for mobile robots or other agents operating within the environment.

- **Problem Objective:** Achieve $(1 - \epsilon) \times 100\%$ coverage of the environment using the minimum number of sensors. This approach reduces the graph size and the complexity of subsequent optimization problems, while also accounting for diminishing returns in complex environments.
- **Constraints:** Defined by the input environment and the visibility model. The environment imposes fundamental visibility and mobility constraints—agents cannot see or move through walls—while the visibility model may introduce additional limitations on visibility, such as a limited sensor range.

We will elaborate on these considerations in greater detail in the following paragraphs.

Our ultimate goal is to enable the construction of route-planning graphs that represent large, complex continuous 2D environments. In these graphs, nodes will represent sensor locations, and edges will denote the shortest paths between them. These graphs will facilitate efficient task-oriented route planning for mobile robots or other agents, including tasks such as inspection, surveillance, monitoring, and searching for objects or targets, all of which require assured sensor coverage.

Throughout this paper, we assume that these graphs will be complete, meaning that every sensor location can be reached from any other sensor location. This assumption applies to connected environments and point agents without kinematic constraints. Therefore, our focus will be solely on determining the graph nodes (sensor locations), which directly addresses the SPP. The edges, if desired, can be constructed using various methods, such as combining visibility graphs [7] with shortest-path algorithms like Dijkstra's [8], or using specialized any-angle path-planning algorithms like Polyanya [9].

While this paper does not specify the exact tasks to be performed on these route-planning graphs, many involve solving NP-hard problems that optimize criteria such as route length, energy consumption, completion time, delivery times, prioritization of specific areas for early inspection, or expected time to find an object or target. Additional constraints may also come into play, such as the capacity of robot batteries and the need for recharging, or the need to avoid collisions in multi-agent scenarios. Examples of such NP-hard problems include the traveling salesperson problem [6], the traveling delivery person problem [10], the graph search problem [11], efficient expected-time mobile search [12], and vehicle routing problems [13]. When specific tasks are not defined, the inherent objective of the SPP is to minimize the graph's size to reduce the complexity of these optimization problems, which aligns with the focus of this paper.

This paper focuses on large and complex environments with numerous intricately shaped obstacles, including narrow passages and concavities, as well as open areas that may require multiple sensor placements. The sheer scale and complexity of these environments render the problem intractable for exact methods as well as some poorly scalable heuristic methods. Additionally, achieving 100% coverage is often impractical due to diminishing returns. In the considered environments,

obtaining 100% coverage can be disproportionately difficult compared to achieving, for example, 99.9% coverage. This difficulty may stem from computational inaccuracies or the inherent complexity of environment boundaries. Furthermore, since the environment representation used for solving the SPP in robotics is a simplified model of a real area, ensuring 99.9% coverage in this simplified representation can be just as effective as 100% coverage for real-world applications. Consequently, we adopt a coverage requirement of $(1 - \epsilon) \times 100\%$, where $\epsilon \in [0, 1]$ is a user-defined constant, typically set to a small value such as 0.001.

To tackle the challenges discussed, we propose the hybrid filtering heuristic (HFH)¹ for the SPP. This heuristic framework enhances the output of an existing sensor-placement method or combines the outputs of multiple methods, incorporating a subsequent filtering step. The goal of the filtering step is to eliminate redundant sensors or sensors that contribute marginally to the coverage, while ensuring that the coverage ratio remains within the interval $[1 - \epsilon, 1]$.

We present two versions of HFH: the basic version, which involves no preprocessing, and a version incorporating a preprocessing technique known as bucketing, originally designed for the point-location problem [14], [15]. We adapt the bucketing technique to accelerate region clipping within the filtering phase, resulting in a variant called HFH with bucketing (HFHB). This version notably improves the runtime of the filtering process. Although based on simple ideas, as illustrated in Fig. 1, an equivalent approach has not, to the best of our knowledge, been proposed and evaluated for the SPP in the literature.

We assess the performance of HFH and HFHB using a dataset of large, complex polygonal environments, considering both unlimited and limited-range omnidirectional visibility models. We compare these methods to several baseline approaches, the majority of which fall into two main categories: random sampling-based and convex partitioning. The results consistently demonstrate that HFH and HFHB outperform the baselines in terms of the number of sensors required to achieve the desired coverage ratio. Additionally, HFHB significantly reduces the runtime of the more competitive baseline methods, making it a viable choice for the application context considered.

Finally, we address scenarios where the sensor's location is subject to uncertainty, such as when the agent cannot guarantee that it will visit the exact sensing location but will instead end up somewhere in its vicinity. This imprecision may arise from localization errors, insufficient precision of the employed actuators or control algorithms, or a combination of these factors. To ensure adequate coverage, we must account for the possibility that the agent could end up at any point within this vicinity. We define the sensor's coverage as the intersection of the visibility regions for all points within this vicinity, which we will refer to as the uncertainty region. In our final set of experiments, we demonstrate that with minimal adaptations,

¹The name HFH reflects its hybrid (H) nature, merging outputs from various sensor-placement methods, implementing a filtering (F) step to remove redundant sensors, and embodying a heuristic (H) approach, which does not guarantee optimality but provides high-quality solutions in practice.

the proposed HFHB method can be applied to such scenarios, up to a certain level of uncertainty, using the same dataset of large, complex polygonal environments.

In summary, the key contributions of this paper are:

- 1) Introduction of the HFH framework for the SPP.
- 2) Development of a filtering step within the HFH framework, utilizing a preprocessing technique known as bucketing, resulting in the HFHB method.
- 3) A comprehensive evaluation of the HFH and HFHB methods in large, complex environments, considering both unlimited and limited-range omnidirectional visibility models, and comparing them against several baseline methods. To the best of our knowledge, the scale of this evaluation—in terms of the size and complexity of the environments—is unprecedented for the SPP.
- 4) Adaptation of the HFHB method to scenarios with localization uncertainty, demonstrating its effectiveness up to a certain level of uncertainty.
- 5) Provision of efficient implementations in for both the proposed and baseline algorithms for polygonal environments. This includes what we believe is the first adaptation of the bucketing technique for fast polygon clipping. The implementations, along with reproduction scripts for the experiments, are available at <https://github.com/janmikulacz/spp>.

The remainder of this paper is organized as follows. Sec. II provides a formal problem statement, outlines the notation used throughout the paper, and includes relevant definitions, including the visibility models considered. Sec. III introduces the HFH framework, detailing the filtering step and the bucketing preprocessing technique. Sec. IV reviews related work, highlighting both the similarities and differences between the proposed approach and existing methods. Sec. V presents a comprehensive computational evaluation of the proposed approach, comparing it with several baseline methods. Finally, Sec. VI concludes the paper and outlines potential directions for future research.

II. PROBLEM FORMULATION AND DEFINITIONS

A. Nomenclature of Sets

In this paper, sets are denoted by normal-font and calligraphic upper-case Roman letters (e.g., A, \mathcal{B}). The notation $|A|$ represents the cardinality of the set A . We use $\{\cdot | \cdot\}$ to indicate set-builder notation, \emptyset to denote an empty set, \setminus for set difference, \cup for set union, and \cap for set intersection. The notation 2^A signifies the power set of A —i.e., the set of all subsets of A including the empty set and A itself.

Furthermore, calligraphic letters (e.g., \mathcal{A}, \mathcal{B}) are employed to represent non-empty, bounded, closed, but not necessarily connected, generally infinite subsets of the Euclidean plane \mathbb{R}^2 , while normal-font letters (e.g., A, B) denote finite sets of varius objects (e.g., numbers, points, or other sets). For the former, $\partial\mathcal{A}$ denotes the boundary of the set \mathcal{A} , $\text{Area}(\mathcal{A})$ represents the area of \mathcal{A} , and $\text{BoundBox}(\mathcal{A})$ denotes the smallest axis-aligned rectangle containing \mathcal{A} . For the latter, $\{a\}$ symbolizes a singleton with the element a , and the expression $a_1 \dots a_n \leftarrow A$ enumerates and indexes all elements

of the set A , where $n = |A|$. The index i of the element $a_i \in A$ is referred to as the ID of a_i .

B. Sensor-Placement Problem (General Formulation)

The sensor-placement problem (SPP) addressed in this paper is defined by a connected environment $\mathcal{W} \subset \mathbb{R}^2$, a visibility model $\text{Vis} : \mathcal{W} \rightarrow 2^{\mathcal{W}}$, and a user-defined uncovered area ratio $\epsilon \in [0, 1]$. Note that the notion of obstacles is implicitly included in the definition of \mathcal{W} , as \mathcal{W} represents the entire see-through space, while its complement, $\mathbb{R}^2 \setminus \mathcal{W}$, represents the opaque space. The visibility model Vis maps a point $p \in \mathcal{W}$ to a set of points $\mathcal{V} \subset \mathcal{W}$ that are visible from p . This set $\mathcal{V} = \text{Vis}(p)$ is called the visibility region of p . The ϵ value determines the maximum permissible ratio of uncovered area within \mathcal{W} .

The SPP aims to determine the minimum finite set of sensor locations within \mathcal{W} such that the area visible by at least one sensor is at least $(1 - \epsilon)$ -times the area of \mathcal{W} , expressed as:

$$\min_{G \in 2^{\mathcal{W}}} |G|, \quad (1)$$

subject to the constraints:

$$|G| \in \mathbb{N}, \quad (2)$$

$$\text{Area}(\bigcup_{g \in G} \text{Vis}(g)) \geq (1 - \epsilon) \text{Area}(\mathcal{W}). \quad (3)$$

Throughout this paper, the set of sensor locations G is referred to as the guard set, and its elements g_1, \dots, g_n , where $n = |G|$, are called guards. The set of guard-visibility region pairs, denoted as $C = \{(g_1, \mathcal{V}_1), \dots, (g_n, \mathcal{V}_n)\}$, where $\mathcal{V}_i = \text{Vis}(g_i)$, is referred to as the coverage of \mathcal{W} by G .

Remark on the Problem Solvability: The preceding formulation, particularly the requirement of a finite guard set G in Eq. (2), assumes that the environment \mathcal{W} and the visibility model Vis are sufficiently well-behaved. As counterexamples, consider an environment with fractal (infinitely complex) boundaries or a visibility model that can only cover a finite number of points, for instance, $\text{Vis}(p) = \{p\}$. In such cases, the minimum guard set may be infinite, making the problem unsolvable. To prevent such pathological cases, we will presume that \mathcal{W} and Vis are sufficiently well-behaved to ensure the problem's solvability throughout this paper. The exact theoretical aspects of the problem's solvability are beyond the scope of this practically oriented paper.

C. Polygonal Environments

The problem defined in the previous subsection and the proposed solution framework introduced later are formulated for general 2D environments with any shape of boundaries, such as polygonal or smooth curves. However, our implementation and evaluation in this paper focus specifically on polygonal environments. A polygonal environment \mathcal{W} is characterized by boundaries consisting of line segments connected to form simple polygons. A polygon is a closed polygonal chain, and simple refers to the property of being strictly non-self-intersecting. The polygonal environment \mathcal{W} has a single outer boundary and zero or more inner boundaries, called holes,

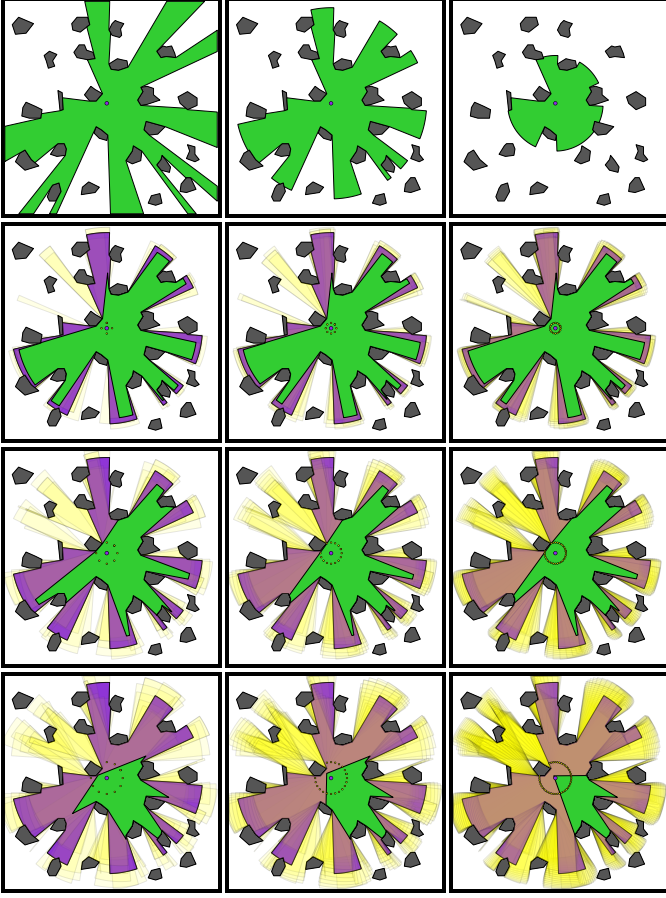


Fig. 2. Various visibility models for the same guard location within a simple $20 \text{ m} \times 20 \text{ m}$ polygonal environment. In all subfigures, the resulting visibility region is filled green, and the guard location is indicated by a violet dot. The first row presents the unlimited visibility model (left) and the limited-range visibility models with $d = 9 \text{ m}$ (center) and $d = 4.5 \text{ m}$ (right). The subsequent rows display the visibility regions for the localization uncertainty visibility model, using a fixed $d = 9 \text{ m}$ while varying r_{samp} (from left to right: $r_{\text{samp}} \approx 0.785 \text{ m}, 0.393 \text{ m}, 0.196 \text{ m}$) and r (from top to bottom: $r = 0.5 \text{ m}, 1.0 \text{ m}, 1.5 \text{ m}$). The samples used to approximate the uncertainty region are marked with yellow dots, and their corresponding visibility regions are represented in semi-transparent yellow. The visibility region of the guard itself is shown in semi-transparent violet.

with all boundaries being pairwise weakly non-intersecting. Weakly non-intersecting means that while the boundaries can touch at isolated points or segments, they cannot cross each other. Technically, if two boundaries share a segment, they can be merged into a single boundary.

D. Visibility Models

This paper considers three visibility models: unlimited visibility, limited-range visibility, and localization uncertainty visibility. In the following paragraphs, we provide a detailed description of each model, along with practical considerations related to clipping operations. Fig. 2 offers a visual guide to the visibility models discussed.

1) *Unlimited Visibility*: The basic visibility model, more specifically the unlimited omnidirectional visibility model, in the polygonal domain is defined as:

$$\text{Vis}(g) = \{p \in \mathcal{W} \mid \overline{gp} \subset \mathcal{W}\}, \quad (4)$$

where \overline{gp} denotes the line segment connecting g and p . The visibility region formed around g is a star-shaped polygon that may have attached one-dimensional antennas [16]. An antenna is created when g aligns with two of the environment's vertices visible from g , imposing constraints on visibility from opposite sides. However, since antennas have zero area, they do not impact coverage quality and can be ignored in the context of the SPP. Therefore, the visibility regions defined by Eq. (4) can be regarded as simple polygons.

Note that in the case of a polygonal environment with no holes, $\epsilon = 0$, and the visibility model defined by Eq. (4), the SPP becomes equivalent to the NP-hard art gallery problem (AGP) [17]. Consequently, the SPP is NP-hard by reduction.

2) *Limited-Range Visibility*: To account for one of the most common limitations in real-world sensor systems, we also consider the limited-range visibility model. In this model, the visibility from a guard g is restricted to a certain distance d (the range), i.e.,

$$\text{Vis}_d(g) = \{p \in \mathcal{W} \mid \overline{gp} \subset \mathcal{W} \text{ and } \|\overline{gp}\| \leq d\}, \quad (5)$$

where $\|\cdot\|$ denotes the Euclidean norm. Note that Vis_∞ is equivalent to Vis from Eq. (4).

3) *Localization Uncertainty*: To address scenarios where the sensor's location is subject to uncertainty, as discussed in the introduction (Sec. I), we introduce the localization uncertainty visibility model. Note that, apart from localization errors, the source of uncertainty may also stem from insufficient precision of the employed actuators or control algorithms, despite the model's name. Under this model, the sensor's location is represented not as a point but as a region. This region is defined by a localization uncertainty model $\text{Unc} : \mathcal{W} \rightarrow 2^{\mathcal{W}}$, which maps a point $p \in \mathcal{W}$ to a set of points $\mathcal{U} \subset \mathcal{W}$. This set $\mathcal{U} = \text{Unc}(p)$ is called the uncertainty region of p . The localization uncertainty visibility model, given a visibility model Vis and an uncertainty model Unc , is defined as the intersection of the visibility regions of all points within the uncertainty region:

$$\text{Vis}_{\text{Unc}}(g) = \bigcap_{u \in \text{Unc}(g)} \text{Vis}(u). \quad (6)$$

In the evaluation, we use a simple uncertainty model with a constant level of uncertainty, which is equivalent to the r -limited visibility model, i.e., $\text{Unc}_r \equiv \text{Vis}_r$. This means the localization error can be expressed in terms of the maximum distance r of the agent's location p from the guard's location g , with the additional constraint that p and g must be visible to each other. This last consideration is very practical, as without it, the uncertainty region might, in the proximity of narrow obstacles, become divided into multiple disconnected parts that are not visible to each other, rendering the visibility region defined by Eq. (6) empty. To complete the definition of the model used in evaluation, we combine Unc_r with the d -limited visibility model, Vis_d , where $d \in (r, \infty]$. The resulting model is denoted as $\text{Vis}_{d, \text{Unc}_r}$. Note that in the absence of obstacles within a distance r from the guard g , the uncertainty region is a circle centered at g with radius r . If the nearest obstacle is at least d away, then the visibility region is also a circle centered at g , but with radius $d - r$. However, when obstacles

are present nearby, the situation becomes more complex, as depicted in Fig. 2.

4) *Practical Considerations Regarding Clipping Operations:* Our implementation of the SPP solution for polygonal environments, regardless of specific details, requires region-clipping operations (note the union in Eq. (3) and the intersection in Eq. (6)). For the unlimited visibility model, where the visibility regions are simple polygons, this process is straightforward due to the availability of established polygon clipping implementations [18].

In contrast, the limited-range visibility model may result in visibility regions with circular arcs, which are more complex to handle. To simplify the clipping of these arcs, we approximate the visibility regions as polygons. This is done by introducing a parameter d_{samp} and sampling each circular arc at equidistant points along its circumference, with a maximum distance $d'_{samp} \leq d_{samp}$ between consecutive samples.

The localization uncertainty visibility model presents even greater challenges, as it involves the intersection of potentially infinitely many visibility regions, which is intractable with existing algorithms, to the best of our knowledge. To address this issue, we use an approximation that considers only a finite number of points within the uncertainty region. These points include the guard itself as well as points sampled along the boundary of the uncertainty region. Specifically, these points are determined through equidistant sampling on a circle of radius r centered at the guard, using a maximum distance of r_{samp} between samples, while discarding any samples that are not visible from the guard.

III. PROPOSED SOLUTION

A. Hybrid Filtering Heuristic (HFH)

This section introduces the hybrid filtering heuristic (HFH) for the SPP. The HFH is not a standalone algorithm; rather, it serves as a framework that extends existing SPP methods or combines multiple methods with a coverage filtering step. This step aims to reduce the number of guards while ensuring that coverage quality remains above a user-defined threshold, assuming the initial guard set meets this requirement.

To clarify, the HFH was designed to be compatible with any SPP methods that generate a finite guard set. The combined output from these methods, referred to as the initial guard set, may or may not satisfy the coverage requirement defined by Eq. (3). If, however, the initial guard set does meet this requirement, the HFH guarantees that the output guard set G also meets it, while reducing guards that do not contribute to the coverage or contribute marginally so that the combined coverage quality remains within the interval $[1 - \epsilon, 1]$. Conversely, if the initial guard set fails to meet the coverage requirement, the HFH maintains the coverage quality at the same level as the initial set while still removing any guards that do not contribute to the coverage at all.

The HFH is outlined in Alg. 1, while its two main concepts—the filtering step and the combination of multiple SPP methods—are illustrated in Fig. 1. The algorithm takes three main inputs: the environment \mathcal{W} , the visibility model Vis , and the allowed uncovered area ratio ϵ . Additionally, the

HFH requires a parameter M , which is a set of SPP methods, each of which takes the same inputs as HFH and returns a finite guard set. Lines 1–3 utilize these methods to generate the initial guard set G . Following this, line 4 prepares the coverage set C for subsequent filtering step at line 5, whose output is returned as the final result at line 6. The FILTERCOVERAGE function implements the filtering step, employing a greedy algorithm to iteratively select guards with the largest residual region area and removing this area from the remaining guards.

To clarify, FILTERCOVERAGE takes the coverage set C along with \mathcal{W} and ϵ as input, generating a new set of filtered guards G . Lines 8–9 unwrap the elements of the coverage set, initializing G as an empty set, the set of remaining IDs L to encompass all initial guard IDs, and the total covered area cov to zero. At this point, the elements of the coverage set are pairs (g_i, \mathcal{V}_i) , where g_i is a guard from the initial set and \mathcal{V}_i is the visibility region of g_i . From this point, a new guard set G is constructed and some guards present in the initial set may not be included in the output. Additionally, the regions \mathcal{V}_i are modified during the filtering process, and are no longer called visibility regions but rather residual regions.

The filtering loop starts at line 10 and continues until the total covered area exceeds $(1 - \epsilon)\text{Area}(\mathcal{W})$ or until L is empty. In each iteration, the guard ID k with the largest residual region area is selected (line 11), and the total covered area is updated (line 12). Subsequently, the residual region of guard k is subtracted from the residual regions of all remaining guards (line 14), and any guard with an empty residual region is removed from L (line 16). Finally, the guard k is added to the output set G (line 17), and the process continues until the termination condition is met.

Algorithm 1 Hybrid Filtering Heuristic (HFH)

Input: Environment $\mathcal{W} \subset \mathbb{R}^2$; visibility model $\text{Vis} : \mathcal{W} \rightarrow 2^\mathcal{W}$; allowed uncovered area ratio $\epsilon \in [0, 1]$.
Parameter: Set of SPP methods M , each taking the input $(\mathcal{W}, \text{Vis}, \epsilon)$ and returning a finite guard set $G \subset \mathcal{W}$.
Output: Finite guard set $G \subset \mathcal{W}$.

- 1: $G \leftarrow \emptyset$
- 2: **for** Method $\in M$ **do**
- 3: $G \leftarrow G \cup \text{Method}(\mathcal{W}, \text{Vis}, \epsilon)$
- 4: $C \leftarrow \{(g, \mathcal{V}) \mid g \in G \text{ and } \mathcal{V} = \text{Vis}(g)\}$
- 5: $G \leftarrow \text{FILTERCOVERAGE}(C, \mathcal{W}, \epsilon)$
- 6: **return** G
- 7: **function** FILTERCOVERAGE(C, \mathcal{W}, ϵ)
- 8: $(g_1, \mathcal{V}_1) \dots (g_n, \mathcal{V}_n) \leftarrow C$
- 9: $G \leftarrow \emptyset; L \leftarrow \{1, \dots, n\}; \text{cov} \leftarrow 0$
- 10: **while** $L \neq \emptyset$ **and** $\text{cov} < (1 - \epsilon)\text{Area}(\mathcal{W})$ **do**
- 11: $k \leftarrow \arg \max_{i \in L} \text{Area}(\mathcal{V}_i)$
- 12: $\text{cov} \leftarrow \text{cov} + \text{Area}(\mathcal{V}_k)$
- 13: **for** $i \in L$ **do**
- 14: $\mathcal{V}_i \leftarrow \mathcal{V}_i \setminus \mathcal{V}_k$
- 15: **if** $\mathcal{V}_i = \emptyset$ **then**
- 16: $L \leftarrow L \setminus \{i\}$
- 17: $G \leftarrow G \cup \{g_k\}$
- 18: **return** G

The computational efficiency of the HFH heavily depends on the implementation of the difference operation at line 14. Alg. 1 illustrates the naïve implementation, which lacks preprocessing and utilizes a slow difference operation that requires the entire \mathcal{V}_k to be clipped from \mathcal{V}_i . Given that this operation occurs in each iteration for every remaining residual region, and considering that the residual regions \mathcal{V}_i and \mathcal{V}_k may potentially be very complex, this naïve implementation is prone to becoming the bottleneck of the HFH. To address this issue, we introduce a bucketing technique that preprocesses the residual regions, accelerating the difference operation and improving the overall performance of the HFH.

B. HFH with Bucketing (HFHB)

To overcome the inefficiency of the naïve implementation, we introduce a faster approach using a technique called bucketing. The resulting method, referred to as HFHB, is outlined in Alg. 2. The bucketing technique involves dividing the environment \mathcal{W} into a grid of square cells, each of side length s , where s is a new parameter. The regions \mathcal{V}_i are then preprocessed into a set of smaller regions B_i by intersecting each \mathcal{V}_i with the grid cells and storing the resulting non-empty intersections as the elements of B_i (lines 3 and 14–23). The subsequent difference operation is then performed on these smaller regions, which are significantly reduced in size and complexity compared to the original regions (lines 9 and 24–34). Moreover, the proposed fast difference operation avoids unnecessary computations by checking whether the regions $\mathcal{B} \in B_i$ and $\mathcal{K} \in B_k$ can intersect (line 28) and only executes the clipping operation if they can (line 29). Otherwise, the unchanged region \mathcal{B} is added to the difference set D (line 33).

The CANINTERSECT function (lines 28 and 35–40) is used to quickly determine whether two regions can intersect by checking whether they belong to the same grid cell (which can be tabulated), whether their bounding boxes intersect (which can be done extremely quickly), and whether the bounding box of the first region intersects with the second region (which is still much faster operation than computing the difference). Note that this function implements a necessary but not sufficient condition for intersection, so the two regions may still not intersect even if this function returns true. However, this is not a problem, as the purpose of this function is to quickly skip over regions that cannot intersect, thereby avoiding the expensive difference clipping operation when it is unnecessary.

IV. RELATED WORK

The original sensor-placement problem, known as the art gallery problem (AGP) [17], is a classic problem in computational geometry. Similar to our formulation, the AGP aims to minimize the number of guards required to cover an environment. However, unlike our formulation, the AGP assumes that the environment is a simple polygon (whereas ours assumes a generic 2D environment), uses an unlimited omnidirectional visibility model (ours is more general), and requires complete coverage (ours allows for a user-defined coverage ratio). In 1975, Chvátal's theorem [17] established that $\lfloor n/3 \rfloor$ guards are

sometimes necessary and always sufficient to guard a simple polygon with n vertices. Since then, numerous related theoretical results have been published, enough to fill a book [19]. For example, it has been demonstrated that the AGP in a polygon with holes is both NP-hard [20], [21] and APX-hard [22].

In practical applications, such as robotic inspection tasks or the design of security and surveillance systems, various visibility constraints may come into play. These constraints might include a limited visibility range or a maximum angle of incidence, adding an extra layer of difficulty. Moreover, dealing with large, complex environments further exacerbates the challenge. As a result, sensor-placement planners often

Algorithm 2 HFH with Bucketing (HFHB)

Add. parameter: Grid cell size $s \in \mathbb{R}^+$ for bucketing.

```

1: function FILTERCOVERAGE( $C, \mathcal{W}, \epsilon$ )
2:    $(g_1, \mathcal{V}_1) \dots (g_n, \mathcal{V}_n) \leftarrow C$ 
3:    $B_1 \dots B_n \leftarrow \text{PREPROCESS}(\mathcal{V}_1 \dots \mathcal{V}_n, \mathcal{W})$ 
4:    $G \leftarrow \emptyset; L \leftarrow \{1, \dots, n\}; \text{cov} \leftarrow 0$ 
5:   while  $L \neq \emptyset$  and  $\text{cov} < (1 - \epsilon)\text{Area}(\mathcal{W})$  do
6:      $k \leftarrow \arg \max_{i \in L} \sum_{\mathcal{B} \in B_i} \text{Area}(\mathcal{B})$ 
7:      $\text{cov} \leftarrow \text{cov} + \sum_{\mathcal{B} \in B_k} \text{Area}(\mathcal{B})$ 
8:     for  $i \in L$  do
9:        $B_i \leftarrow \text{DIFFERENCE}(B_i, B_k)$ 
10:      if  $B_i = \emptyset$  then
11:         $L \leftarrow L \setminus \{i\}$ 
12:       $G \leftarrow G \cup \{g_k\}$ 
13:    return  $G$ 
14: function PREPROCESS( $\mathcal{V}_1 \dots \mathcal{V}_n, \mathcal{W}$ )
15:    $(\mathcal{C}_{11} \dots \mathcal{C}_{1w}) \dots (\mathcal{C}_{h1} \dots \mathcal{C}_{hw}) \leftarrow \text{Grid}(\mathcal{W}, s)$ 
16:   for  $i \leftarrow 1 \dots n$  do
17:      $B_i \leftarrow \emptyset$ 
18:     for  $x \leftarrow 1 \dots w$  do
19:       for  $y \leftarrow 1 \dots h$  do
20:          $\mathcal{B} \leftarrow \mathcal{V}_i \cap \mathcal{C}_{xy}$ 
21:         if  $\mathcal{B} \neq \emptyset$  then
22:            $B_i \leftarrow B_i \cup \{\mathcal{B}\}$ 
23:   return  $B_1 \dots B_n$ 
24: function DIFFERENCE( $B, K$ )
25:    $D \leftarrow \emptyset$ 
26:   for  $\mathcal{B} \in B$  do
27:     for  $\mathcal{K} \in K$  do
28:       if CANINTERSECT( $\mathcal{B}, \mathcal{K}$ ) then
29:          $\mathcal{D} \leftarrow \mathcal{B} \setminus \mathcal{K}$ 
30:         if  $\mathcal{D} \neq \emptyset$  then
31:            $D \leftarrow D \cup \{\mathcal{D}\}$ 
32:         else
33:            $D \leftarrow D \cup \{\mathcal{B}\}$ 
34:   return  $D$ 
35: function CANINTERSECT( $\mathcal{B}, \mathcal{K}$ )
36:   if GridCell( $\mathcal{B}$ ) = GridCell( $\mathcal{K}$ ) then
37:     if BoundBox( $\mathcal{B}$ )  $\cap$  BoundBox( $\mathcal{K}$ )  $\neq \emptyset$  then
38:       if BoundBox( $\mathcal{B}$ )  $\cap$   $\mathcal{K} \neq \emptyset$  then
39:         return true
40:   return false

```

rely on approximation or heuristic approaches, which we will discuss next.

In the robotics community, González-Baños and Latombe conducted highly influential research on a variant of the SPP [23], [24]. They proposed two randomized sampling methods aimed at covering the boundary of a polygonal environment with the fewest number of guards. These methods considered constraints on minimum and maximum visibility range, as well as the maximum angle of incidence. Although their focus was on boundary coverage and included additional constraints, these methods can be seamlessly adapted to cover the entire environment and solve the SPP formulation presented in this paper.

The first approach involves extensive random sampling of the input environment until complete boundary coverage is achieved. The subsequent objective is to identify the minimum subset of these samples that still achieves complete coverage. In this stage, the boundary is divided into maximal connected components, each of which can be fully covered by a particular subset of guards. These components are then labeled with unique identifiers, forming the set called the universe U . A family S of subsets of U is then created, where each subset corresponds to a single guard and its elements represent the component labels covered by that guard. The goal is to identify the smallest subfamily $C \subset S$ whose union is U . This problem is known as the minimum set cover problem (MSCP) and is one of the classic NP-hard problems identified by Karp in 1972 [25]. Besides being NP-hard, the MSCP is also known to be APX-hard [26]. Despite the notorious difficulty of MSCP, González-Baños and Latombe proposed using a greedy algorithm. A well-studied variant of the greedy algorithm selects the set that covers the largest number of uncovered components in each iteration [27].

According to González-Baños and Latombe, the aforementioned approach has two main flaws that may limit its practical usability: a quadratic dependency on the number of samples and the potential redundancy of many samples due to unsystematic random sampling. To address these issues, the authors introduced an alternative incremental approach, which is their second method. This method involves sampling the constraints of the problem (points on the boundary) rather than the entire environment and incorporates the dual sampling (DS) scheme. Initially, the DS scheme selects a point on the uncovered part of the boundary and determines the visible region from that point. This region is then sampled with dual samples, and the dual sample that covers the largest portion of the uncovered boundary is added to the partial solution. This iterative process continues until the desired level of coverage is achieved. It is evident that, instead of just the boundary, this approach can be used to cover the entire environment, which is the main focus of our work.

In addition to sampling-based heuristic methods, several convex-partitioning heuristics have also been proposed for the SPP. These methods partition the input environment into disjoint convex regions (disjoint except at their boundaries), each of which can be completely covered by a single guard. For example, the constrained conforming Delaunay triangulation (CCDT) [28] is a method that generates a triangular mesh of

the underlying polygonal environment based on the Delaunay triangulation of a set of points in the plane. In CCDT, the mesh is constrained by the environment's boundaries and conforms to a set of user-defined constraints. For the limited-range visibility model, these constraints correspond to the maximum radii of the triangles' circumcircles. For the unlimited visibility model, no additional constraints are imposed, resulting in the constrained Delaunay triangulation (CDT). Guards are then placed at the circumcenters of all acute triangles and at the midpoints of the bases of all obtuse triangles.

Kazazakis and Argyros [29] introduced a different heuristic tailored for the limited-range visibility model. This iterative method begins with a convex polygonal mesh of the input environment, which can be constructed, for example, by merging the triangles of the CDT. The method then iteratively subdivides the convex polygons to create a finer mesh that adheres to the limited-range visibility constraint. Guards are positioned within each resulting polygon by calculating the weighted average of the midpoints of the polygon's edges, with the weights determined by the lengths of the edges.

Additionally, we consider a method that does not fall into the previously mentioned categories. This method is as simple as placing guards at all the reflex vertices of the environment (or a single guard anywhere if the environment is convex). This approach was suggested in [12] to achieve complete coverage under the unlimited visibility model in the context of robotic search tasks. However, we found no formal proof confirming that this method guarantees complete coverage in a polygon with holes. There is a related result for simple polygons showing that placing guards at all reflex vertices ensures complete coverage [30]. Another result from [19] implies that placing guards at all convex vertices guarantees coverage of a simple polygon's exterior. A proof of the discussed method's sufficiency for polygons with holes could build on these results. Specifically, it might be shown that coverage is guaranteed in a hole-free polygon by placing guards at all reflex vertices, and adding a hole with guards at its convex vertices (which are reflex with respect to the polygon with the hole) should not reduce coverage. We conjecture that such a proof could be valid, but formalizing it is beyond the scope of this paper. For now, we confirm that this method works for all evaluation instances.

Now we will discuss the HFH framework proposed in this paper and its relation to the previously mentioned approaches. The HFH framework revisits the concept of transforming the SPP into the MSCP, which is then solved by a greedy algorithm. However, it significantly differs from the first method suggested by González-Baños and Latombe. First, instead of random sampling, the initial guard set is generated more systematically using a set of initial SPP methods. These methods should be selected to be as fast as possible while ensuring that their combined output provides coverage of the desired quality. As we show later in the computational evaluation, selecting more methods to generate diverse initial guard sets can lead to a smaller guard set after filtering, though this comes at the cost of increased computational time. The second main difference is that the HFH framework does not explicitly compute the universe U and the family S sets.

Instead, the greedy algorithm used in the filtering step selects guards based on the maximum uncovered area they cover. Note that this selection strategy differs from the maximum-cardinality set cover strategy used in the MSCP's greedy algorithm and is more similar to the incremental approach of the DS scheme. However, the HFH framework also differs from the DS scheme in that it does not use dual samples. The set of samples is predetermined by the initial SPP methods, which allows for preprocessing and acceleration strategies like the bucketing technique. Furthermore, the convex-partitioning methods and the reflex-vertices method can be employed as initial SPP methods within the HFH framework. In conclusion, the HFH framework integrates ideas from all the mentioned approaches into a unique solution strategy.

Finally, let us consider the option of extending the HFH framework with a more sophisticated filtering step. This option naturally arises when realizing that the MSCP solution strategy is not limited to the greedy algorithm. On the other hand, greedy algorithms are generally simple and fast, which is a significant advantage in practice. As we show in the computational evaluation, the greedy algorithm employed in the HFH framework provides the best trade-off between computational time and solution quality compared to the SPP baseline algorithms discussed in this section. However, this does not mean that other filtering strategies are not worth exploring. Although we consider this to be beyond the scope of this paper, we believe that some of the more recent metaheuristics for the MSCP, surveyed and compared in [31], could be adapted to the SPP and integrated into the HFH framework. We leave this as a potential direction for future research.

V. COMPUTATIONAL EVALUATION

A. Evaluation Metrics

The performance of any SPP method can be evaluated based on three main metrics: the number of returned guards $n = |G|$, the total computational time t needed to compute the final guard set, and the ratio of the environment covered by at least one guard:

$$\%CR = \frac{\text{Area} \left(\bigcup_{g \in G} \text{Vis}(g) \right)}{\text{Area}(\mathcal{W})} \times 100\%. \quad (7)$$

However, if the evaluated method guarantees complete coverage or a coverage quality of at least $(1 - \epsilon) \times 100\%$, the last metric becomes non-informative and is omitted from the evaluation unless explicitly stated otherwise.

Comparing methods based solely on the number of guards n can be challenging due to high variance across different problem instances. Therefore, we introduce an alternative relative metric, the percentage best-known solution gap $\%BG(n) \in [0, \infty)$, which measures the relative difference between the number of guards n returned by a method and the best-known solution n_{best} for the specific instance:

$$\%BG(n) = \frac{n - n_{best}}{n_{best}} \times 100\%. \quad (8)$$

The value n_{best} is determined by identifying the minimum number of guards recorded across all evaluated methods

TABLE I
MAP PROPERTIES.

Map	<i>n</i>	<i>h</i>	<i>x</i>	<i>y</i>	<i>xy</i>	<i>a</i>	Pre
2p01	1909	140	189	210	39,606	31,484	
2p02	1428	137	270	270	72,889	53,909	
2p03	2347	153	330	310	102,300	58,924	✓
2p04	998	52	240	310	74,389	52,758	
4p01	2919	274	320	320	102,387	75,312	
4p02	3799	315	380	502	190,605	109,607	✓
4p03	4838	300	400	410	163,984	97,727	
6p01	3558	234	368	498	183,584	121,713	
6p02	3419	214	400	440	175,792	130,409	✓
6p03	2464	229	500	500	249,980	151,745	
cha01	1357	112	230	280	64,390	41,997	✓
cha02	2108	101	335	570	190,932	176,227	
cha03	3462	320	400	430	171,983	99,653	
cha04	4688	407	440	440	193,582	120,911	
endmaps	4923	340	565	770	435,023	360,408	
pol01	959	51	323	133	42,798	12,839	
pol02	3296	239	470	515	242,030	96,545	
pol03	4118	394	420	510	214,181	127,080	
pol04	3978	268	350	340	118,986	72,535	✓
pol05	2860	239	515	395	203,198	85,389	
pol06	5315	465	470	480	225,581	156,673	✓
rus01	2331	134	331	224	73,976	33,160	
rus02	1337	72	242	307	74,455	31,114	
rus03	3463	295	450	430	193,482	69,337	✓
rus04	3198	265	338	500	169,100	104,296	
rus05	3459	220	404	419	169,285	84,142	✓
rus06	5145	383	545	455	247,955	111,825	
rus07	2147	137	460	380	174,783	85,189	
sax01	1583	127	380	485	184,283	78,603	
sax02	4448	255	403	634	255,845	117,736	✓
sax03	2827	143	416	462	192,381	86,305	
sax04	4639	286	585	675	394,850	139,834	
sax05	1623	54	445	420	186,883	86,215	
sax06	2524	163	405	465	188,308	96,977	
sax07	2758	165	310	340	105,387	69,180	✓

Legend: n : no. vertices; h : no. holes; x : map width; y : map height; xy : bounding box area; a : map area; Pre: ✓ if used only in the preliminary evaluation.

and their individual runs for the specific instance (non-deterministic methods are run multiple times to account for randomness). Note that the gap is computed using on the best-known solution provided by one of the evaluated (heuristic) methods. It is not based on the optimal solution, which remains unknown for our large-scale instances due to their intractability.

B. Benchmark Instances

The SPP instance consists of the polygonal environment \mathcal{W} , the visibility model Vis, and the allowed uncovered area ratio ϵ , which is fixed at 0.001 for all experiments.

The polygonal environments used in this paper are derived from a dataset of 35 polygonal maps from the videogame Iron Harvest, developed by KING Art Games, as introduced in [32]. These maps typically span across 400×400 meters and are characterized by thousands of vertices and dozens to hundreds of holes. They were specifically chosen for their significant scale and complexity. To ensure the environments are well-formed, we preprocessed the maps to create connected polygons with holes that are free of self-intersections and overlapping holes, while ensuring a minimal representation (i.e., no redundant vertices). The preprocessing involved a sequence of



Fig. 3. Showcase of the visibility models used in the evaluation on the 2p01 map. In all images, the guard location is the same and marked with a yellow dot. The left image displays the unlimited visibility model Vis_{∞} and the range-limited visibility models Vis_d with $d = 64, 32, 16, 8, 4 m stacked on top of each other in this order, gradually changing the color from blue for Vis_{∞} to red for Vis_4 . Stacking the models in this way retains all information, as each model is a subset of the one before it in the sequence. The middle image shows a similar scene but with the localization uncertainty visibility model $\text{Vis}_{\infty,\text{Unc}_r}$ using $r = 0.1, 0.2, 0.4, 0.8, 1.6 m, changing the color from blue to cyan. The right image presents the same for $\text{Vis}_{16,\text{Unc}_r}$, transitioning from purple for Vis_{16} to green for $\text{Vis}_{16,\text{Unc}_{1.6}}$.$$

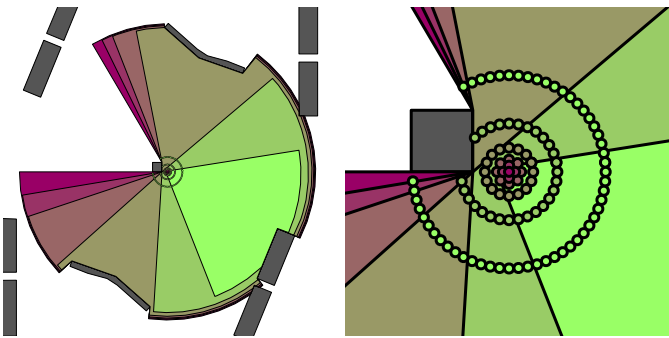


Fig. 4. Detailed views of the right image from Fig. 3, showcasing the visibility models Vis_{16} and $\text{Vis}_{16,\text{Unc}_r}$ with $r = 0.1, 0.2, 0.4, 0.8, 1.6 m. In these views, the guard location has been replaced by the samples used to approximate the visibility regions. For Vis_{16} , a single sample, shown in purple, represents the guard. In the other models, additional samples are displayed in their corresponding colors, forming rings at the r distance from the guard, as illustrated in the right image. Recall that the color of the regions and samples transitions from purple to green as localization uncertainty increases.$

smoothing operations: applying the Ramer-Douglas-Peucker (RDP) algorithm [33] with a tolerance of 0.1 m, performing inflation and deflation operations with a radius of 0.2 m, and finally inflating again with a radius of 0.01 m before applying the RDP algorithm with a tolerance of 0.1 m. After these steps, we finalized the preprocessing by selecting the largest polygon from the refined representation and incorporating all enclosed holes, while discarding any additional disconnected artifacts, such as polygons that are not connected to the main polygon with holes or those fully enclosed within the holes. The properties of the resulting maps are summarized in Tab. I.

The visibility models used in the evaluation include the unlimited visibility model Vis_{∞} , the range-limited visibility

model Vis_d with $d \in \{4, 6, 8, 12, 16, 24, 32, 48, 64, 96, 128\}$ m, and the localization uncertainty visibility model $\text{Vis}_{d,\text{Unc}_r}$ with $r \in \{0.1, 0.2, 0.4, 0.8, 1.6\}$ m, using the same d values as those for Vis_d . The sampling parameter d_{samp} has been chosen such that for the smallest d value, $d = 4$, the visibility region in open space (i.e., in the absence of nearby obstacles) is approximated by a 12-sided regular polygon: $d_{\text{samp}} = \frac{4 \cdot 2\pi}{12} \text{ m} \approx 2.094 \text{ m}$. Similarly, the sampling parameter r_{samp} has been selected to ensure that for the smallest non-zero r value, $r = 0.1$, there are at least 4 samples (plus 1 for the guard) to approximate the visibility region under the localization uncertainty model: $r_{\text{samp}} = \frac{0.1 \cdot 2\pi}{4} \text{ m} \approx 0.157 \text{ m}$. For details on the models, including the exact meaning of these parameters, recall Sec. II-D.

To illustrate the scale and complexity of the benchmark instances and to demonstrate that the parameters of the visibility models were chosen reasonably, we present visualizations of the 2p01 map and the visibility models in Fig. 3, along with a detailed view in Fig. 4. Note that this selected map is relatively small and not overly complex, with 1,909 vertices, 140 holes, and a total area of 31,484 m². In comparison, the largest map in the dataset by area, endmaps, has 4,923 vertices, 340 holes, and a total area of 360,408 m², while the largest map by number of vertices, pol06, has 5,315 vertices, 465 holes, and a total area of 156,673 m².

C. Baseline Methods

We evaluate the proposed HFH and HFHB methods against a set of baseline methods, detailed below.

- 1) RV [12]: A method that places guards at the reflex vertices of the polygonal environment \mathcal{W} , ensuring complete coverage under the unlimited visibility model Vis_{∞} .
- 2) CCDT [28]: A convex-partitioning method that ensures complete coverage under the range-limited visibility

model Vis_d . This method generates a triangular mesh of \mathcal{W} that adheres to the maximum circumcircle radius constraint, placing guards at the circumcenters of acute triangles and at the base midpoints of obtuse triangles.

- 3) KA [29]: Another specialized convex-partitioning method designed for the range-limited visibility model Vis_d .
- 4) RS: A basic random sampling method that uniformly samples the environment \mathcal{W} and places guards at these sampled points until the desired coverage quality, as determined by Eq. (3), is achieved.
- 5) IRS: An informed random sampling method that, unlike RS, maintains and updates the uncovered region, placing guards at uniform samples drawn specifically from this region until the desired coverage quality is achieved.
- 6) DS k [24]: A dual sampling method that places a new guard by drawing a uniform sample from the uncovered region and computing a visibility region \mathcal{V} from this sample. Then, $k \in \mathbb{N}$ additional (dual) samples are drawn from \mathcal{V} , and the one covering the largest area of the uncovered region is chosen as the new guard. Here, k serves as a parameter for this method, and the variant using a fixed k value is denoted as DS k - k (e.g., DS k -10 for $k = 10$).
- 7) DS ρ : An alternative parameterization of DS with a fixed density of samples $\rho \in \mathbb{R}^+$. Under this parameterization, the number of dual samples within \mathcal{V} is computed as $k = \lceil \rho \cdot \text{Area}(\mathcal{V}) \rceil$. The variant using a fixed ρ value is denoted as DS ρ - ρ (e.g., DS ρ -0.1 for $\rho = 0.1$).

For a complete background on these methods, refer to Sec. IV.

D. Method Parameterizations

The proposed HFH and HFHB methods are parameterized by the set of guard methods M . Additionally, HFHB is parameterized by the cell size s for bucketing. For the unlimited visibility model Vis_∞ , we consider 7 variants of M prescribed by $2^A \setminus \{\emptyset\}$, where $A = \{\text{KA}, \text{CCDT}, \text{RV}\}$, representing three of the baseline methods. These specific methods were chosen because they are fast and guarantee complete coverage without utilizing ϵ , allowing the filtering step to remove guards that contribute marginally to the coverage. For the range-limited visibility model Vis_d , we use the same options except for $M = \{\text{RV}\}$, as the RV method alone does not guarantee complete coverage under this model. The cell size for HFHB is set to $s = 0.1 \cdot \max(x, y)$, where x and y are the width and height of \mathcal{W} , respectively.

The baseline method DS k is evaluated using the following parameter values: $k \in \{2, 4, 8, 16, 32, 64, 128, 256\}$. Its alternative parameterization DS ρ is evaluated with $\rho \in \{0.02, 0.04, 0.08, 0.16, 0.32, 0.64, 1.28, 2.56\}$. The remaining baseline methods are parameter-free.

E. Implementation Details

The proposed and baseline methods were implemented in C++, utilizing a shared codebase that includes essential components for computing triangular meshes and visibility regions, performing polygon clipping, and conducting map preprocessing operations.

Triangular meshes are computed using Triangle² [28], [34], which relies on Delaunay refinement algorithms introduced in [35], [36] and supports user-defined constraints such as the maximum circumcircle radius, as detailed in Sec. IV. Visibility regions are computed using the visibility library Trivis³ [37] developed by the authors of this paper and introduced in [38]. This library is based on the triangular expansion algorithm proposed in [16] and supports both unlimited and range-limited visibility models, with the latter representing output as a sequence of line segments and circular arcs. However, as mentioned in Sec. II-D, our codebase currently lacks support for arc-clipping, so these circular arcs are approximated by line segments during clipping operations. Polygon clipping and preprocessing operations are executed using Clipper2⁴, which builds upon and significantly extends the Vatti clipping algorithm [39].

The implementation is single-threaded, compiled in Release mode using GCC compiler version 12.3.0, and executed on a personal laptop, the Lenovo Legion 5 Pro 16ITH6H, with an Intel Core i7-11800H processor (4.60GHz), 16GB of RAM, and running Ubuntu 20.04.6 LTS. The source code, including the reproduction scripts for the experiments, is available at <https://github.com/janmikulacz/spp>.

F. Other Evaluation Details

The evaluation is conducted in three stages that differ in purpose, methodology, and results presentation: preliminary, main, and additional.

The purpose of the preliminary stage is to obtain initial insights into the performance of all proposed and baseline methods and to identify representative methods for a more thorough evaluation in the main stage, with a primary focus on the unlimited and limited-range visibility models. Since this stage aims to compare a large number of methods broadly, we use only two aggregated metrics: the mean number of guards \bar{n} and the mean computational time \bar{t} .

The main stage aims to deliver stronger and more detailed results for the representative methods through a comprehensive evaluation. It seeks to conduct a detailed comparison between the proposed methods and the baseline methods, again focusing on the unlimited and limited-range visibility models. As this stage aims to compare the methods in more detail, we provide complete statistics in the form of boxplots for the number of guards n . To reduce variance across different maps and visibility models, we use the relative version of the metric %BG(n), defined in Eq. (8).

The additional stage intends to provide further insights into the performance of a single proposed method under the localization uncertainty visibility model. In this context, the method does not guarantee the required coverage quality, so we include a third metric, the percentage covered ratio %CR, defined in Eq. (7).

The preliminary stage considers all the proposed and baseline methods, parameterized as described in Sec. V-D, totaling

²Available at <https://www.cs.cmu.edu/~quake/triangle.html>.

³Available at <https://github.com/janmikulacz/trivis>.

⁴Available at <https://github.com/AngusJohnson/Clipper2>.

39 versions, with only 9 selected for the main stage. To follow best practices in computational evaluation, as the preliminary stage resembles a form of parameter tuning, the benchmark instances are split into two disjoint subsets: 10 maps for the preliminary stage and 25 maps for the main and additional stages, as indicated in Tab. I. To make both the experimental load and the results presentation more manageable, the preliminary stage uses a reduced set of d values: $d \in \{\infty, 64, 32, 16, 8\}$ m.

In all experiments, the non-deterministic methods (RS, IRS, DS k , and DS ρ) are executed 10 times for each instance using different random seeds to account for their inherent randomness. The remaining methods are deterministic, so each instance is solved only once.

G. Preliminary Results

The preliminary results are presented in Fig. 5, showcasing the performance of all proposed and baseline methods. To aid in interpreting these results, we define method a_1 as dominating method a_2 if a_1 achieves lower values for both aggregated metrics, \bar{n} and \bar{t} . We particularly focus on methods that are not dominated by any other method, which are indicated by pink circles in the plots.

Among the baseline methods, KA, IRS, and DS k -2 are the most frequently marked as non-dominated (KA appears 4 times, IRS and DS k -2 appear 3 times each). We select KA and IRS for the main evaluation. KA is noted for its speed but also exhibits significant quality gaps, while IRS demonstrates more balanced performance. DS k -2 is not selected as it represents a DS method with very few dual samples and is thus very similar to IRS.

Among the proposed methods, HFHB-KA, HFHB-KA,RV, and HFHB-KA,CCDT,RV each achieve non-dominated status the maximum number of times (5 times). For the main evaluation, we select HFHB-KA,CCDT,RV for its minimal number of guards and HFHB-KA,RV for its favorable trade-off between the two metrics. We also include their respective HFH versions to examine the impact of bucketing on performance.

Next, we consider the remaining DS methods, which are only occasionally marked as non-dominated, particularly when the number of dual samples is small and the visibility radii are larger. Despite this, they remain important baselines. It is noteworthy that as the number of dual samples in DS methods increases, their solution quality improves but eventually plateaus, while their computational costs rise significantly. Additionally, the DS k parametrization is generally more effective than the DS ρ parametrization. This may be because smaller visibility regions require denser dual samples to achieve a lower number of guards. These smaller visibility regions often indicate a higher density of nearby obstacles, leading to more complex and varied visibility regions from the dual samples, thus requiring denser dual samples to discover the ones that cover most of the uncovered region.

As a result, we exclude the DS ρ methods from the main evaluation and choose DS k -16, DS k -64, and DS k -256 to represent the DS method with moderate, high, and very high sample counts, respectively. We do not include DS methods with smaller sample counts since IRS already represents the same principle using a single sample.

H. Main Results

The main results are presented in Fig. 6, showcasing the performance of the 9 representative methods. We will first comment on the performance of the baseline methods and then discuss the proposed methods.

Among the baseline methods, KA stands out significantly as the fastest, being the fastest method overall. Its mean runtime, \bar{t} , is close to zero for all visibility models. However, KA also exhibits the poorest solution quality, with the mean $\%BG(n)$ around 667% for the unlimited visibility model, decreasing to 77% for the limited radius of 4 m.

The sampling methods aim to balance runtime and solution quality based on the number of dual samples used. IRS, using only one sample and no dual samples, emerges as the fastest among them, though it has the poorest solution quality, with mean $\%BG(n)$ values starting at 70% for Vis_{∞} and decreasing to 9% for $d = 4$. DS k -16, DS k -64, and DS k -256, using 16, 64, and 256 dual samples respectively, start with mean $\%BG(n)$ values of 20%, 14%, and 9% for Vis_{∞} , decreasing to 3%, 2%, and 1% for $d = 4$, respectively.

As expected, runtime increases with a larger number of dual samples, while solution quality improves. However, the quality improvement seems to approach a plateau, as suggested by the plots and more clearly observed in the preliminary results in Fig 5. Thus, more dual samples do not necessarily lead to a significant improvement in solution quality. Additionally, the runtime of all sampling methods reaches its minimum for medium visibility radii (around $d = 24$) and increases in both directions from that point. The runtime increase for larger visibility radii can be attributed to the higher costs of computing visibility regions, which are generally larger and more complex. The runtime increase for smaller visibility radii is due to the need for more guards to cover the same area, combined with the increased cost of maintaining the uncovered region. Note that while the area of the uncovered region decreases with each new guard, its complexity in terms of the number of vertices can temporarily increase (until it is reduced to almost nothing towards the end) as many small regions are clipped away.

The proposed methods, HFH and HFHB, exhibit the best solution quality among all tested methods. For the KA,CCDT,RV variant, the mean $\%BG(n)$ is close to 0% for all visibility models, and less than 4% for the KA,RV variant. No other methods consistently achieve such low values, except for the DS methods under the smallest visibility radius. Additionally, HFHB variants are notably faster than their corresponding versions without bucketing. Fig. 7 shows the average percentage reduction in runtime for the HFHB methods compared to the HFH methods. The reduction in runtime is most significant for $d = 24$: 25.4% for the KA,CCDT,RV variant and 23.8% for the KA,RV variant. These reductions correspond to approximately a 4-fold speedup.

Overall, HFHB-KA,RV provides the best trade-off between runtime and solution quality, as it consistently finds fewer guards compared to all baseline methods while being faster than the most competitive sampling methods, DS k -64 and DS k -256. For $d < 16$, it is also faster than IRS and DS k -16,

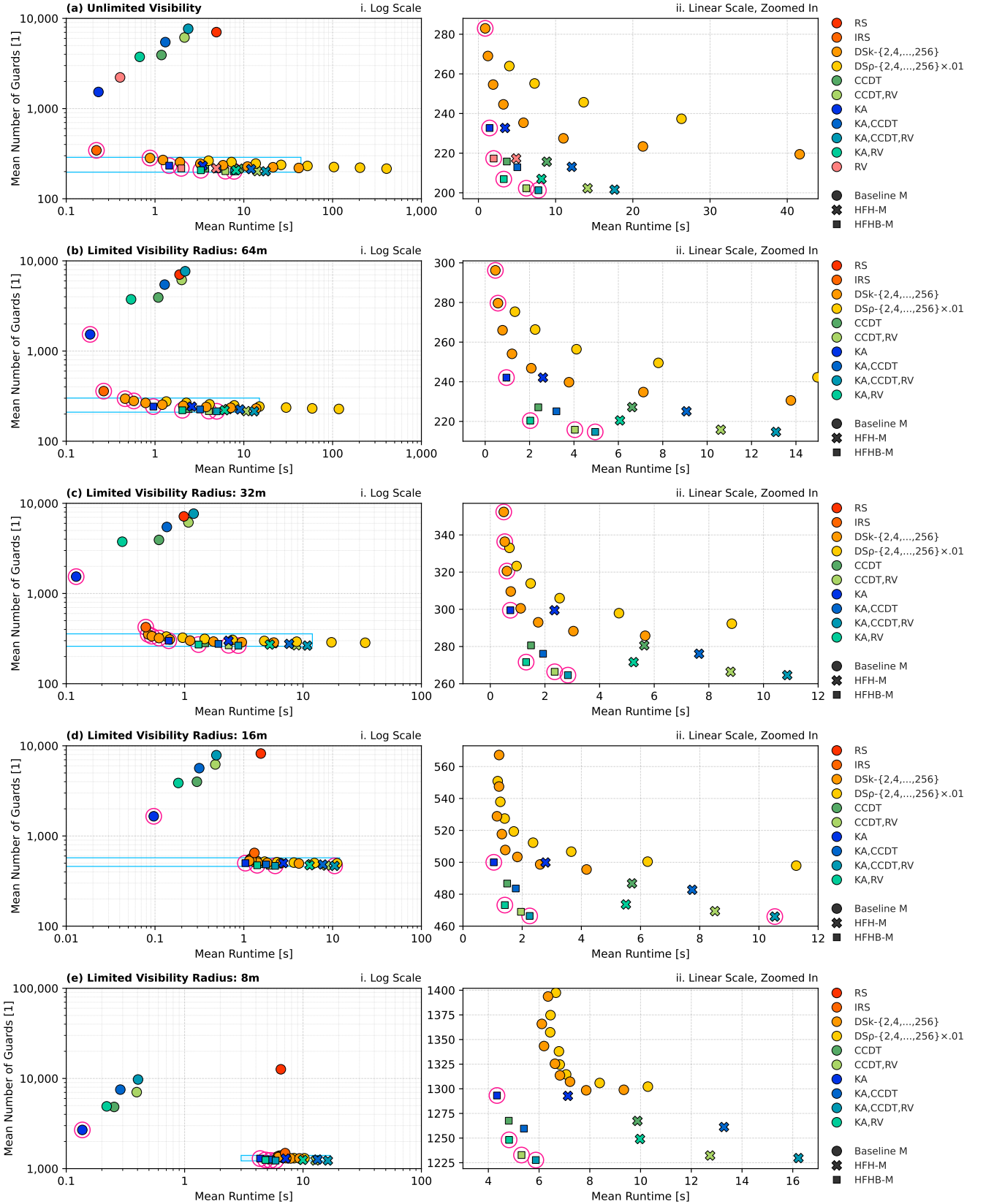


Fig. 5. The preliminary results for 5 selected visibility models and all 39 methods. Each row of plots corresponds to a specific visibility model: the top for the unlimited visibility model Vis_{∞} , and the remaining for the range-limited visibility models Vis_d with $d = 64, 32, 16, 8$ m. The left column displays the results in log scale, whereas the right column presents the results in linear scale, zoomed into the blue-shaded region shown in the left column. Each point in the scatterplots represents a single method and is defined as (\bar{t}, \bar{n}) , where \bar{t} is the mean computational time and \bar{n} is the mean number of guards, aggregated over all 10 maps in the preliminary subset and all 10 runs for the non-deterministic methods. The marker shape indicates the type of method: a circle for baseline methods, a cross for the HFH method, and a square for the HFHB method. The marker color represents a specific set of baseline methods, as shown in the legend. Methods that are not dominated by any other method are marked with pink circles.

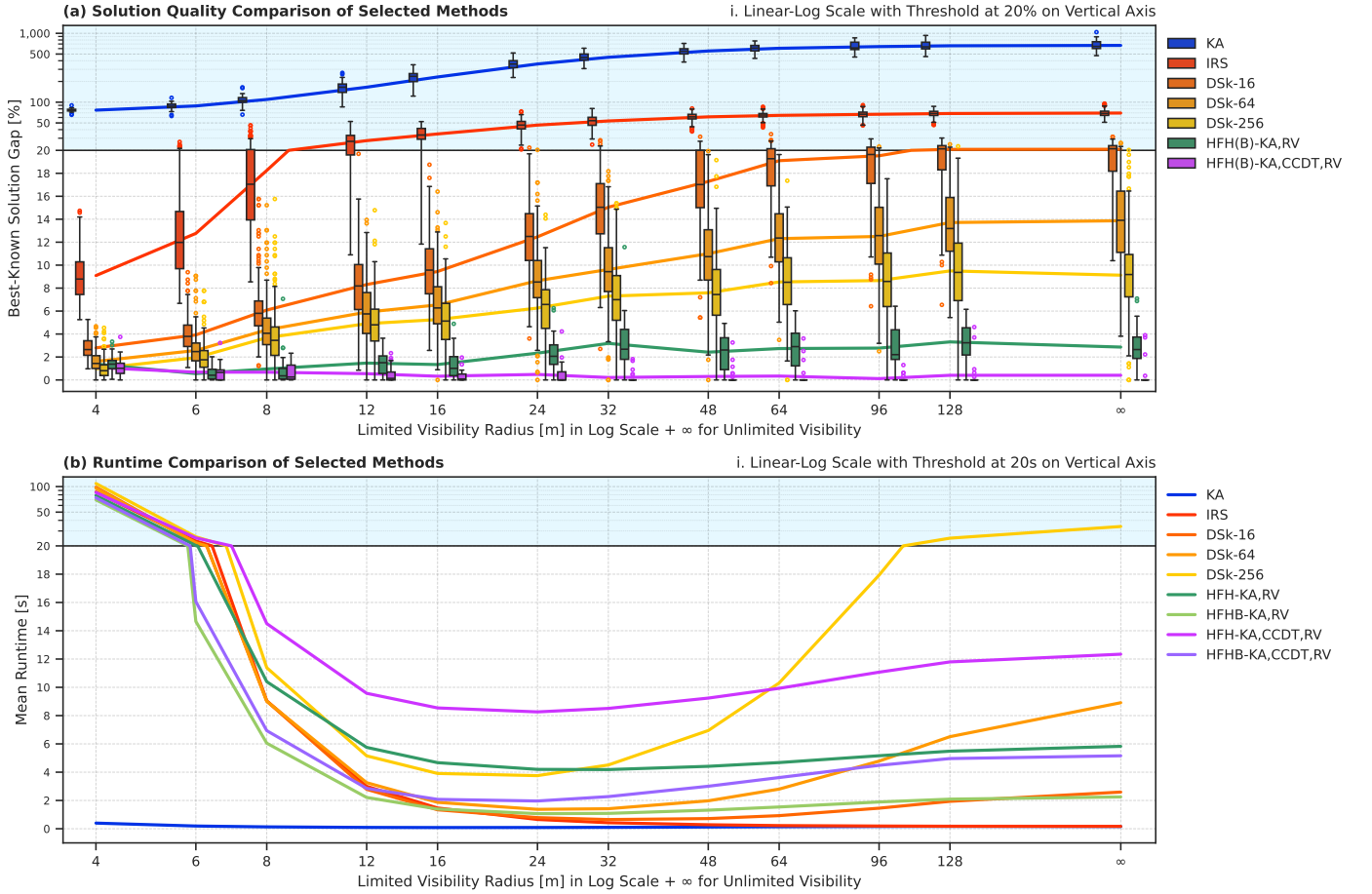


Fig. 6. The main results for all 11 limited-range visibility models, plus one for Vis_{∞} , and the 9 representative methods. The top plot shows the solution quality comparison in terms of the percentage best-known solution gap $\%BG(n)$, while the bottom plot displays the runtime comparison in terms of runtime t . The line plots represent the mean values for each method, while the boxplots show the distribution of metric values across all 25 maps in the main subset and all 10 runs for the non-deterministic methods. For clarity, the boxplots for runtime are omitted due to high variance across all methods, caused by dataset variability. For the quality comparison, the HFHB methods are merged with their respective HFH methods, as they provide statistically equivalent results (aside from minor differences due to numerical inaccuracies). In both plots, the lower portion is in linear scale, while the upper portion is in log scale, as indicated by the shaded region.

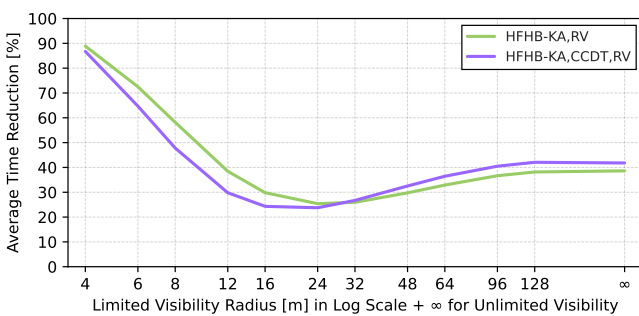


Fig. 7. Average percentage reduction in runtime for the HFHB method compared to the HFH method without bucketing. In the plot, the runtime of the HFH method corresponds to 100%.

and for $d > 16$, it has a mean runtime below 2.25 seconds. The KA,CCDT,RV variant further reduces the number of guards (by more than 2% for $d > 24$) but at the cost of a slightly higher runtime (more than twice as high for $d > 24$). For $d < 24$, the relative differences between the two variants are

progressively less pronounced.

I. Additional Results

The additional results examine the performance of the HFHB-KA,RV method under the localization uncertainty visibility model $\text{Vis}_{d,\text{Unc}_r}$. Recall that HFH(B)-M only guarantees the desired coverage ratio if the input methods set M guarantees it. In the case of $\text{Vis}_{d,\text{Unc}_r}$, we do not have such a guarantee, as neither KA, RV, nor their combination ensures the desired coverage ratio. However, we can still evaluate the practical performance of HFHB-KA,RV by including a third metric: the percentage covered ratio (%CR), defined in Eq. (7).

Additionally, we introduce minor adaptations to KA and RV for the localization uncertainty visibility model to improve coverage quality. The KA adaptation uses a radius of $d - r$ instead of d as input to the method. This adjustment is motivated by the fact that, in the absence of nearby obstacles, the localization uncertainty visibility model produces a circle with radius $d - r$. The RV adaptation involves moving the guards along the reflex vertex axis by a distance of $r + 10^{-6}$ away from the vertex, unless this would place the guard

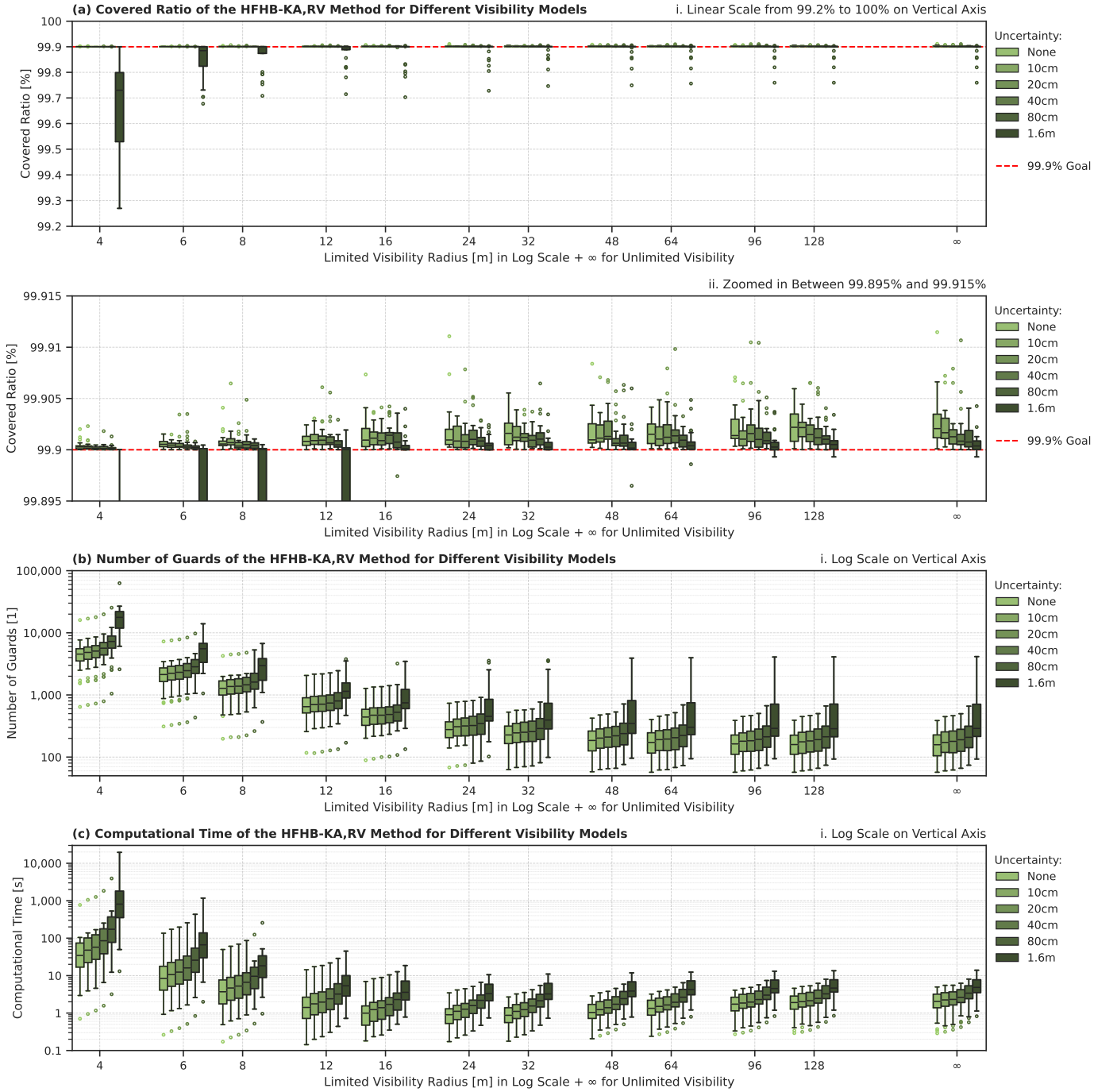


Fig. 8. The additional results for the adapted HFHB-KA,RV method under the localization uncertainty visibility model $\text{Vis}_{d,\text{Unc},r}$. The boxplots illustrate the distribution of metric values across all 25 maps in the main subset. Each boxplot corresponds to a specific visibility model with different d and r values, as indicated by the horizontal axis labels for d and the colors, which are explained in the legend, for r . The first plot shows the covered ratio %CR in the range [99.2, 100]%. The second plot zooms in on the range [99.895, 99.915]% to provide a more detailed view. The dashed red line in both plots represents the coverage ratio goal of $(1 - \epsilon) \times 100\% = 99.9\%$. The third and final plots show the number of guards n and runtime t , respectively, both in log scale.

beyond the environment boundary. This approach addresses the issue where guards close to obstacles experience significant reductions in their visibility regions under the localization uncertainty model, as illustrated in Fig. 4. This adaptation mitigates such reductions, increasing the likelihood that the guard will contribute effectively to coverage and be retained during the filtering step.

The results are presented in Fig. 8. The most notable observation is that the adapted HFHB-KA,RV method consistently achieves the desired coverage ratio of 99.9% for $r \leq 0.4$ m across all d values. For $r = 0.8$ m, there is a single instance where the coverage ratio falls below 99.9% (the outlier for $d = 16$ m). For $r = 1.6$ m, the coverage ratio is often below 99.9%, with the lowest recorded instance around 99.2% for $d = 4$ m. In conclusion, the adapted HFHB-KA,RV method empirically achieves the desired coverage ratio for small to moderate localization uncertainty radii but struggles with larger radii. The number of guards and runtime primarily serve as informational metrics in this context and are generally higher for larger r values and smaller d values, as expected.

VI. CONCLUSIONS AND FUTURE WORK

In conclusion, this paper introduces the hybrid filtering heuristic (HFH) and its accelerated variant, HFHB, for addressing the sensor-placement problem (SPP) in complex 2D environments. HFH combines different placement methods with a filtering step to minimize sensor count while maintaining user-defined coverage quality. HFHB enhances this approach with bucketing for faster region clipping. Our results show that HFHB outperforms traditional methods, offering practical solutions for complex environments and demonstrating promising adaptation to localization uncertainty.

Future work will focus on applying HFHB to visibility-related route-planning tasks, such as efficient inspection and search in polygonal environments. Additionally, we will explore more realistic localization uncertainty models and develop sensor-placement methods with coverage guarantees under these models, to be integrated into HFHB.

REFERENCES

- [1] A. T. Murray, K. Kim, J. W. Davis, R. Machiraju, and R. Parent, “Coverage optimization to support security monitoring,” *Computers, Environment and Urban Systems*, vol. 31, no. 2, pp. 133–147, 2007.
- [2] J. Kritter, M. Brévilliers, J. Lepagnot, and L. Idoumghar, “On the optimal placement of cameras for surveillance and the underlying set cover problem,” *Applied Soft Computing*, vol. 74, pp. 133–153, 2019.
- [3] W. Ostachowicz, R. Soman, and P. Malinowski, “Optimization of sensor placement for structural health monitoring: a review,” *Structural Health Monitoring*, vol. 18, no. 3, pp. 963–988, 2019.
- [4] W. An, S. Ci, H. Luo, D. Wu, V. Adamchuk, H. Sharif, X. Wang, and H. Tang, “Effective sensor deployment based on field information coverage in precision agriculture,” *Wireless Communications and Mobile Computing*, vol. 15, no. 12, pp. 1606–1620, 2015.
- [5] M. P. Vitus and C. J. Tomlin, “Sensor Placement for Improved Robotic Navigation,” in *Robotics: Science and Systems VI*, Y. Matsuoka, H. Durrant-Whyte, and J. Neira, Eds. The MIT Press, 2011, pp. 217–224.
- [6] J. Faigl, M. Kulich, and L. Přeučil, “A Sensor Placement Algorithm for a Mobile Robot Inspection Planning,” *Journal of Intelligent & Robotic Systems*, vol. 62, no. 3-4, pp. 329–353, 2011.
- [7] M. de Berg, M. van Kreveld, M. Overmars, and O. C. Schwarzkopf, “Visibility Graphs,” in *Computational Geometry: Algorithms and Applications*. Springer, 2000, pp. 307–317.
- [8] E. W. Dijkstra, “A note on two problems in connexion with graphs,” *Numerische Mathematik*, vol. 1, no. 1, pp. 269–271, 1959.
- [9] M. Cui, D. D. Harabor, and A. Grastien, “Compromise-free pathfinding on a navigation mesh,” in *Proceedings of the Twenty-Sixth International Joint Conference on Artificial Intelligence*. AAAI, 2017, pp. 496–502.
- [10] J. Mikula and M. Kulich, “Solving the traveling delivery person problem with limited computational time,” *Central European Journal of Operations Research*, vol. 30, no. 4, pp. 1451–1481, 2022.
- [11] M. Kulich, L. Přeučil, and J. J. Miranda Bront, “On multi-robot search for a stationary object,” in *2017 European Conference on Mobile Robots (ECMR)*. IEEE, 2017, pp. 1–6.
- [12] A. Sarmiento, “Generating expected-time efficient trajectories for rapidly finding an object in known environments,” Ph.D. dissertation, University of Illinois at Urbana-Champaign, 2004.
- [13] D. G. Macharet and M. F. M. Campos, “A survey on routing problems and robotic systems,” *Robotica*, vol. 36, no. 12, pp. 1781–1803, 2018.
- [14] T. Asano, “A new point-location algorithm and its practical efficiency: comparison with existing algorithms,” *ACM Transactions on Graphics*, vol. 3, no. 2, pp. 86–109, 1984.
- [15] D. Fišer, J. Faigl, and M. Kulich, “Growing neural gas efficiently,” *Neurocomputing*, vol. 104, pp. 72–82, 2013.
- [16] F. Bungiu, M. Hemmer, J. Hershberger, K. Huang, and A. Kröller, “Efficient Computation of Visibility Polygons,” 2014, arXiv:1403.3905.
- [17] V. Chvátal, “A combinatorial theorem in plane geometry,” *Journal of Combinatorial Theory, Series B*, vol. 18, no. 1, pp. 39–41, 1975.
- [18] A. Johnson, “Clipper2—A Polygon Clipping and Offsetting library (C++)”
- [19] J. O’Rourke, *Art Gallery Theorems and Algorithms*. Oxford University Press, 1987.
- [20] J. O’Rourke and K. Supowit, “Some NP-hard polygon decomposition problems,” *IEEE Transactions on Information Theory*, vol. 29, no. 2, pp. 181–190, 1983.
- [21] D. Lee and A. Lin, “Computational complexity of art gallery problems,” *IEEE Transactions on Information Theory*, vol. 32, no. 2, pp. 276–282, 1986.
- [22] S. Eidenbenz, C. Stamm, and P. Widmayer, “Inapproximability Results for Guarding Polygons and Terrains,” *Algorithmica*, vol. 31, no. 1, pp. 79–113, 2001.
- [23] H. González-Baños and J.-C. Latombe, “Planning Robot Motions for Range-Image Acquisition and Automatic 3D Model Construction,” in *AAAI Fall Symposium Series*. AAAI, 1998.
- [24] H. González-Baños, “A randomized art-gallery algorithm for sensor placement,” in *Proceedings of the seventeenth annual symposium on Computational geometry*. ACM, 2001, pp. 232–240.
- [25] R. M. Karp, “Reducibility among Combinatorial Problems,” in *Complexity of Computer Computations*. Springer US, 1972, pp. 85–103.
- [26] U. Feige, “A threshold of $\ln n$ for approximating set cover,” *Journal of the ACM*, vol. 45, no. 4, pp. 634–652, jul 1998.
- [27] V. Chvatal, “A Greedy Heuristic for the Set-Covering Problem,” *Mathematics of Operations Research*, vol. 4, no. 3, pp. 233–235, 1979.
- [28] J. R. Shewchuk, “Delaunay refinement algorithms for triangular mesh generation,” *Computational Geometry*, vol. 22, no. 1-3, pp. 21–74, 2002.
- [29] G. Kazazakis and A. Argyros, “Fast positioning of limited-visibility guards for the inspection of 2D workspaces,” in *IEEE/RSJ International Conference on Intelligent Robots and System*, vol. 3. IEEE, 2002, pp. 2843–2848.
- [30] J. Urrutia, “Art Gallery and Illumination Problems,” in *Handbook of Computational Geometry*. Elsevier, 2000, pp. 973–1027.
- [31] L. Rosenbauer, A. Stein, H. Stegherr, and J. Hähner, “Metaheuristics for the Minimum Set Cover Problem: A Comparison,” in *Proceedings of the 12th International Joint Conference on Computational Intelligence*. SCITEPRESS, 2020, pp. 123–130.
- [32] D. Harabor, R. Hechenberger, and T. Jahn, “Benchmarks for Pathfinding Search: Iron Harvest,” in *Proceedings of the International Symposium on Combinatorial Search*, vol. 15, no. 1, 2022, pp. 218–222.
- [33] D. H. Douglas and T. K. Peucker, “Algorithms for the reduction of the number of points required to represent a digitized line or its caricature,” *Cartographica: The International Journal for Geographic Information and Geovisualization*, vol. 10, no. 2, pp. 112–122, 1973.
- [34] J. R. Shewchuk, “Triangle: Engineering a 2D Quality Mesh Generator and Delaunay Triangulator,” *Applied Computational Geometry Towards Geometric Engineering*, vol. 1148, pp. 203–222, 1996.
- [35] L. P. Chew, “Guaranteed-quality mesh generation for curved surfaces,” in *Proceedings of the ninth annual symposium on Computational geometry - SCG ’93*. ACM Press, 1993, pp. 274–280.

- [36] J. Ruppert, “A Delaunay Refinement Algorithm for Quality 2-Dimensional Mesh Generation,” *Journal of Algorithms*, vol. 18, no. 3, pp. 548–585, 1995.
- [37] J. Mikula and M. Kulich, “TříVis: Versatile, Reliable, and High-Performance Tool for Computing Visibility in Polygonal Environments,” in *IEEE/RSJ International Conference on Intelligent Robots and Systems*. IEEE, 2024, manuscript accepted for publication.
- [38] ——, “Optimizing Mesh to Improve the Triangular Expansion Algorithm for Computing Visibility Regions,” *SN Computer Science*, vol. 5, no. 2, p. 262, 2024.
- [39] B. R. Vatti, “A generic solution to polygon clipping,” *Communications of the ACM*, vol. 35, no. 7, pp. 56–63, 1992.